Numerical simulation of the spatio-temporal development of linear disturbances in Stokes layers: Absolute instability and the effects of high frequency harmonics

Alexander Ramage
College of Engineering, Swansea University, Bay Campus, Swansea, SA1 8EN, UK

Christopher Davies*
School of Mathematics, Cardiff University, Cardiff, CF24 4AG, UK

Christian Thomas
Department of Mathematics and Statistics, Macquarie University, New South Wales, 2109, Australia

Michael Togneri
College of Engineering, Swansea University, Bay Campus, Swansea, SA1 8EN, UK

For a family of oscillatory Stokes layers, the spatio-temporal evolution of impulsively excited disturbances is investigated, using direct numerical simulations of the linearised Navier–Stokes equations. The semi-infinite planar Stokes layer is modified to incorporate a low-amplitude, high-frequency harmonic, which provides a simplified model of the external noise found in physical experiments. For the unmodified Stokes layer, impulsively excited disturbances are known to form family-tree-like structures, composed of multiple wavepackets. The long-term behaviour that is encompassed within these structures is studied, together with the effects upon them of the alterations to the base flow. In the absence of any base-flow modification, the disturbances are discovered to exhibit a subharmonic pattern of temporal growth, with a periodicity that is twice that of the basic state. It is also shown that when linear instability first arises, it takes an absolute rather than a convective form. Inclusion of a high-frequency harmonic into the basic state is found to have a strong and destabilising impact upon the impulse response. The development of the family-tree-like disturbance structure can be disrupted, changing the character of the absolute instability and promoting its appearance at much reduced Reynolds numbers.

I. INTRODUCTION

The current study is concerned with numerical simulations of the linear stability behaviour for a relatively simple set of time-periodically unsteady shear flows. The flows investigated are taken from a family of oscillatory boundary layers which are all generated by the time-periodic motion of an infinitely long and flat rigid plate, placed beneath an otherwise stationary body of viscous fluid. They are straightforward enough to be described by exact analytic solutions to the Navier–Stokes equations, and may thus be considered to provide paradigm examples for the promotion of conceptual understanding for time-periodic flows. The simplest possible case, where the periodic motion of the bounding wall is prescribed to be entirely sinusoidal, and hence characterised by a single temporal frequency, is what is usually called the Stokes layer. Herein, to limit the possibilities

* DaviesC9@cardiff.ac.uk

for ambiguity, this will often be referred to as being the *pure* or *monochromatic* Stokes layer. It provides the starting point for our investigations, but these will then be extended to configurations where the time variation of the base flow is altered to a weakly non-sinusoidal form.

Periodic flows have the analytical advantage that Floquet theory can be applied to obtain equations that determine the disturbance development. Infinitesimal perturbations from a time-periodic shear flow may be decomposed into modes with the general form $\exp(i\alpha x + \mu t)f(t, y)$, where x is the direction along which the flow oscillates, α is the corresponding modal wavenumber, y is the direction of the shear and the function f is time-periodic with the same period as the basic state. The real part of the Floquet exponent μ characterises the net growth or decay displayed by the perturbations from one time period of the flow oscillation to the next. A crucial alteration from the normal mode form that is deployed for the case of steady shear flows is that the time-periodic function f will in general comprise a multitude of temporal frequencies, rather than displaying a purely sinusoidal variation. Much of this paper will be taken up with the surprisingly complex issue of how superpositions of such Floquet modes of disturbance can evolve over both space and time. In particular, we will use numerical simulations to study the long-term behaviour of the specific combinations which are picked out by a localised form of impulsive disturbance forcing. As might be expected, Floquet theory proves to be very helpful in interpreting our results. However, the impulse response can turn out to be far more elaborate and interesting than might have been anticipated from the consideration of any individual Floquet mode in isolation [1].

Mainly because the required computational resources were not initially available, there was a two decade interval between the first attempt [2] to use Floquet theory to complete a numerical study of the linear stability of the pure Stokes layer and the eventual determination of the instability threshold [3]. The prediction for the onset of unstable behaviour at a critical Reynolds number $Re_c \sim 700$ has subsequently been confirmed by other independently conducted studies [4–6]. With the results of the Floquet theory providing guidance, direct numerical simulations were deployed to investigate the spatial-temporal evolution of disturbance wavepackets, formed in response to an impulsively applied excitation [1]. These simulations revealed an intriguing, and completely unexpected, family-tree-like structure, which involved the successive birthing of multiple wavepackets. Newly discovered features of this intricate disturbance structure will be reported here, alongside an account of its disruption when the periodicity of the underlying flow is no longer taken to be monochromatic.

The stability results that were obtained from Floquet theory, for the case of the monochromatic Stokes layer, appear to be very disparate with what has been reported in physical experiments. Although linear instability is predicted to set in for $Re_c \sim 700$, many empirical studies detected unstable behaviour at much lower values, with $Re \sim 300$ being typical [7–10]. In order to address this discrepancy, a slight alteration of the basic state was modelled [11], by adding a low-amplitude, high-frequency harmonic to the motion of the bounding wall. This aimed to capture an imperfection that was present in the experiments, where the mechanical generation of the wall motion introduced low level noise into what was intended to be a purely sinusoidal oscillation. Though it is difficult, retrospectively, to accurately quantify the noise that had been persistent, high-frequency modulation was reported to have amounted to as much as 1% of the amplitude of the oscillatory wall motion [7, 9]. When this modulation was represented in the Floquet stability analysis by the incorporation of a high frequency harmonic into the basic state, with a matching magnitude of order 1%, it was discovered that the critical Reynolds number could be decreased by more than a half [11], bringing it much more in line with the experimental observations.

Such remarkable quantitative shifts in the predictions of the Floquet stability theory, when there is only a small alteration of the basic state, motivated us to conduct a numerical investigation to ascertain the effect upon the family-tree-like disturbance structures that develop in the spatial-

temporal plane. Although the flow regimes modelled herein are similar to those investigated by Thomas et al [11], numerical simulations allow us to make new insights into the behaviour of disturbances that was not possible using linear stability analysis.

As has already been indicated, our concern here will be with the impulse response for perturbations developing in both the pure Stokes layer and for the family of flows where the motion of the oscillating plate has been modified by a low-amplitude, high-frequency oscillation. Three features are of particular interest: the family-tree-like structure associated with the development of multiple wavepackets; the temporal growth or decay of the disturbance maximum; and the long-time temporal behaviour of the disturbance at fixed spatial locations. Consideration of the latter aspect allows us to categorise disturbances as being either convectively or absolutely unstable [12]. Newly developed numerical algorithms, in conjunction with the availability of high-performance computational resources, facilitated a considerable extension in the scope of the results that we were able to obtain.

The remainder of this paper is outlined as follows. An overview of the formulation and the numerical scheme is presented in §2. In §3 and §4, simulation results are discussed for both the pure and the modified Stokes layers. Firstly, very clear evidence is given for the absolute instability of the pure Stokes layer. The effects of low-amplitude, high-frequency harmonics are then described. Finally, conclusions are drawn in §5.

II. FORMULATION

A. Base flow

Consider the two-dimensional flow that develops in a semi-infinite region of viscous incompressible fluid, bounded by a flat plate located in the plane $y = 0$ that oscillates along this plane with a time-periodic motion. The co-ordinate axes are aligned so that the plate movement takes place only along the streamwise x-direction, while the y-axis represents the direction normal to the bounding plate. The wall velocity U_w is comprised of a fundamental oscillation of frequency ω, modified by some low-amplitude, high-frequency harmonic, exactly as for the previously conducted Floquet analysis [11]. It is expressed as

$$U_w = U_s \left[\cos(\omega t) + \delta \left(a_p \cos(p\omega t) + b_p \sin(p\omega t)\right)\right], \tag{1}$$

where p is a positive integer. The parameter pair (a_p, b_p) dictates the relative phase of the harmonic. The normalisation $a_p^2 + b_p^2 = 1$ is adopted, so that δ represents a measure of the noise amplitude. The case $\delta = 0$ corresponds to the classical Stokes layer which, as has already been mentioned, will also be referred to here as either the pure or the monochromatic Stokes layer.

All velocity fields are non-dimensionalised by the amplitude of the fundamental oscillation U_s and we use the non-dimensional time variable $\tau = \omega t$. Units of length are scaled with the Stokes layer thickness associated with the fundamental oscillation, $d = \sqrt{2\nu/\omega}$, where ν is the kinematic viscosity of the fluid. The Reynolds number can then be defined as $Re = U_s/\sqrt{2\nu\omega}$. Given these scalings, the non-dimensional basic state takes the form

$$\boldsymbol{U} = (U_B(y,\tau), 0, 0),$$

where

$$U_B(y,\tau) = \mathrm{e}^{-y}\cos(\tau - y) + \delta \mathrm{e}^{-\sqrt{p}y}\left[a_p \cos(p\tau - \sqrt{p}y) + b_p \sin(p\tau - \sqrt{p}y)\right]. \tag{2}$$

B. Discretisation of the disturbance governing equations

Disturbances to the basic state (2) are investigated through direct numerical simulations, conducted using a velocity-vorticity form of the linearised Navier–Stokes equations [13]. The perturbations are assumed to be sufficiently small to permit the linearisation of the governing equations through the removal of non-linear terms. Since Squire's theorem can be extended to temporally periodic flows [14], we may restrict our investigation to two-dimensional perturbations. The total velocity and vorticity fields are thus expressed as

$$(U, V) = (U_B, 0) + (u, v) \quad \text{and} \quad \Omega = \Omega_B + \zeta, \tag{3a,b}$$

where $\Omega_B = U_B'$ is the undisturbed vorticity associated with the base flow U_B (a prime denotes differentiation with respect to y). Perturbation fields u and v represent the streamwise and wall-normal velocities, while ζ denotes the corresponding vorticity perturbation.

A spectral treatment of the variation along the streamwise direction is implemented, whereby disturbances are decomposed into Fourier components of the form

$$\{u, v, \zeta\}(x, y, \tau) = \{u_j, v_j, \zeta_j\}(y, \tau) \exp(i\alpha_j x) + \text{c.c.}, \tag{4}$$

where $\alpha_j = j\Delta\alpha$ for $j = 0 \ldots J-1$ specifies a discrete set of wavenumbers with a fixed increment $\Delta\alpha$ and c.c. denotes the complex conjugate. The evolution of each such component of the total disturbance can be independently determined, because the streamwise homogeneity of the basic state and the linearity of the governing equations leads to their decoupling. The disturbance development that ensues from imposing a localised impulsive forcing, with a prescribed temporal variation and streamwise distribution, can be reconstructed by taking an appropriate superposition. Some further details of this are given below. It may be noted that the wavenumber increment $\Delta\alpha$ establishes a $2\pi/\Delta\alpha$-spatial periodicity, which must always be taken to be large enough to enclose the streamwise spreading of any physically significant perturbations that develop over the time duration considered in a given numerical simulation. In particular, care needs to be taken to avoid the creation of disturbance artificialities that might otherwise arise from encroachments upon the boundaries of the computational domain. The upper wavenumber limit $\alpha_{up} = (J-1)\Delta\alpha$ also needs to be well-chosen, to ensure that there is sufficient resolution of the smallest features of the streamwise variation. In practice, it was found that taking $\alpha_{up} = 0.6$ gave satisfactory results, since Fourier components with higher values of the wavenumber were found to be subject to a rapid temporal decay which made their contribution physically insignificant.

For each of the selected values of α_j the two-dimensional version of the velocity-vorticity formulation for the linearised Navier–Stokes equations [1, 13] yields a vorticity transport equation for ζ_j and a Poisson equation for v_j

$$\frac{1}{Re}\frac{\partial \zeta_j}{\partial \tau} + i\alpha_j U_B \zeta_j + U_B'' v_j = \frac{1}{2Re}\left(\frac{\partial^2}{\partial y^2} - \alpha_j^2\right)\zeta_j, \tag{5a}$$

$$\left(\frac{\partial^2}{\partial y^2} - \alpha_j^2\right) v_j = -i\alpha_j \zeta_j. \tag{5b}$$

The streamwise velocity perturbation field u_j may then be specified via the integral expression

$$u_j = -\int_y^\infty (\zeta_j + i\alpha_j v_j)\, \mathrm{d}y, \tag{5c}$$

although calculation of this quantity is not explicitly required in order to conduct the simulations that compute the disturbance evolution. Note that for the nondimensionalisation used here, the unsteady term is scaled with the viscous terms. This is consistent across many studies of oscillatory flows [1, 3, 11] but differs from the scaling usual for steady flows, in which the $1/Re$ term is absent.

The disturbance is impulsively forced via the introduction of a small temporally and spatially localised vertical displacement of the bounding wall. The corresponding linearised boundary conditions are implemented through the no-slip and no-penetration conditions

$$u_j(0,\tau) = -U_B'(0,\tau)\eta_j(\tau) \quad \text{and} \quad v_j(0,\tau) = \frac{\partial \eta_j}{\partial \tau}. \tag{6a,b}$$

An integral constraint on ζ_j is then derived by coupling (5c) and (6a) to give

$$\int_0^\infty \zeta_j \, \mathrm{d}y = U_B'(0,\tau)\eta_j(\tau) - \int_0^\infty i\alpha_j v_j \, \mathrm{d}y. \tag{7}$$

The latter is derived from the previously specified expression that yields the streamwise velocity component. Each of the time-dependent variables η_j represents a Fourier component from the decomposition of the wall displacement. All disturbances are assumed to vanish in the limit $y \to \infty$.

In physical space, the localised impulsive forcing is prescribed by setting

$$\eta(x,\tau) = \mathrm{e}^{-\lambda_f x^2}(1 - \mathrm{e}^{-\sigma\tau^2})\,\mathrm{e}^{-\sigma\tau^2} \simeq \frac{1}{J}\sum_{j=0}^{J-1} \eta_j(\tau)\,\mathrm{e}^{i(j\Delta\alpha)x}. \tag{8}$$

The parameter σ is used to characterise the time duration of the forcing and λ_f determines its range along the streamwise direction. It may be noted that, without any loss of generality, the impulsive excitation can be taken to be centred about $x = 0$, since the base flow does not vary with the streamwise co-ordinate. For $\tau \gg 1/\sqrt{\sigma}$ we have, in effect, an undisplaced wall with $\eta = 0$. Through the use of an appropriate discrete Fourier transform, the relationship between $\eta(x,\tau)$ and the set of Fourier coefficients $\eta_j(\tau)$ can be inverted to determine the excitation that is to be imposed on each of the independently evolving modes that comprise the total disturbance.

The wall-normal variation of the disturbances is discretised using a novel numerical method [15] in which the y-derivatives are approximated by fourth-order compact finite-differences [16] applied with respect to a computational co-ordinate ξ. The semi-infinite domain $y \in [0,\infty)$ is mapped on to $\xi \in (0,1]$ via the algebraic transformation $\xi = s/(y+s)$, where s is a stretching factor that specifies the distribution of the physical grid points across the boundary layer. The temporal evolution is determined using an implicit-explicit predictor-corrector time-stepping scheme.

Once numerical solutions have been obtained for the Fourier components of the disturbance for each wavenumber $\alpha_j \in [0, \alpha_{up}]$, they can be readily transformed into quantities that vary only with respect to the physical space and in time. For example, for any given streamwise position x, the perturbation vorticity at the discretisation point where $y = y_k, \tau = \tau_l$ may be determined from the computed set of values $\zeta_j(y_k,\tau_l)$ using the superposition

$$\zeta(x,y_k,\tau_l) = \sum_{j=0}^{J-1} \zeta_j(y_k,\tau_l)\mathrm{e}^{i(j\Delta\alpha)x}. \tag{9}$$

The streamwise grid was usually chosen with $x = x_j = j\Delta x$, where $\Delta x = L/J$ and $L = 2\pi/\Delta\alpha$ is the size of the previously mentioned periodicity in the computational domain. This permitted the deployment of Fast Fourier Transforms to evaluate the required superpositions.

Because the perturbations associated with each streamwise wavenumber α_j evolve completely independently of each other, our numerical simulation method naturally lends itself to code parallelisation. The computational time durations for the simulations were thus substantially reduced by utilising multiple processors. Further details concerning the implementation of this, together with a much fuller account of all of our numerical procedures, can be found in [17].

It may be noted that for any chosen value of α_j, the long-term behaviour of the corresponding Fourier component, as determined by numerically solving the given system of governing equations for ζ_j and v_j, would be expected to be dominated by the most unstable Floquet mode with that particular wavenumber. This has the consequence that its eventual temporal growth should be predictable from results that can be obtained entirely from the Floquet theory. Careful checks were undertaken to confirm that this was actually the case for a representative set of wavenumbers and Reynolds numbers.

C. Temporal growth rates and depiction of spatial-temporal evolution

Although we will not replicate here the previously reported Floquet stability analysis [11] for the family of base flows given by (2), it is informative to consider the temporal structure which it presupposes. This has the general form

$$F(x, y, \tau) = \mathrm{e}^{\mu\tau} f(x, y, \tau), \tag{10}$$

where f is 2π-periodic in τ (i.e. shares the periodicity of the basic state) and F represents some disturbance field. The real part of the complex Floquet exponent μ determines the temporal growth. It measures the change in the amplitude of F at 2π intervals.

The presumed form for the temporal variation can be readily deployed to derive recipes to compute growth rates from the simulation data. These recipes may then be applied when interpreting the response to a spatially localised impulsive excitation; even though this will be comprised of a superposition of different Floquet modes, characterised by a range of wavenumbers. Measures of the growth rate $\mu_r = \mathbb{R}\{\mu\}$ were in practice computed from the simulation data obtained for the wall vorticity $\zeta(x, 0, \tau)$, although other choices were found to give similar results. The temporal growth associated with the disturbance maximum was calculated using the formula

$$\mu_m(\tau) = \frac{1}{2\pi} \ln \left(\sqrt{1 + \frac{2\pi}{\tau}} \frac{\max_x |\zeta(x, 0, \tau + 2\pi)|}{\max_x |\zeta(x, 0, \tau)|} \right), \tag{11}$$

while the growth about a fixed spatial location x_0 was computed from

$$\mu_0(\tau) = \mathbb{R} \left\{ \frac{1}{2\pi} \ln \left[-\sqrt{1 + \frac{4\pi}{\tau}} \, \frac{\Im[\zeta(x_0, 0, \tau + 4\pi)/\zeta(x_0, 0, \tau + 2\pi)]}{\Im[\zeta(x_0, 0, \tau)/\zeta(x_0, 0, \tau + 2\pi)]} \right] \right\}. \tag{12}$$

In the subsequent study, the temporal growth rate about a fixed streamwise location will be referred to as the *pointwise* growth rate. The stated formulae (11)-(12) are derived by fitting ζ to the anticipated Floquet evolution (10) with more detailed justification provided in [17]. A similar approach for measuring growth rates was implemented in an earlier study [1]. The square root factors, which involve a division by τ, are brought in to take account of the $\sqrt{\tau}$ algebraic modification to the exponential growth that is usually required when describing boundary layer wavepacket development. After sufficient time has passed, (11) is used to distinguish between stable ($\mu_m < 0$)

and unstable ($\mu_m > 0$) disturbances. Using (12), unstable disturbances can be further categorized as convectively or absolutely unstable. Convective instability describes an unstable disturbance that is convected out of any region of interest and is therefore characterised by pointwise decay ($\mu_0 < 0$) whereas absolute instability is charactersized by pointwise growth ($\mu_0 > 0$) at every spatial location the disturbance reaches.

Spatial-temporal contour plots of the values taken by the envelope of the wall vorticity perturbations $|\zeta(x, 0, \tau)|$ will also be utilised to facilitate the investigation of the evolution of the disturbances. No special significance should be attached to the use of the wall vorticity as a means of presenting the evolution of disturbances. This particular perturbation field was also utilised by [1], and as a matter of consistency we present results using this quantity. Equivalent observations and conclusions would be drawn if alternative quantities were used. These contour plots illustrate the multiple wavepacket structures that develop in response to the impulsive forcing and can help to identify whether the disturbances are convectively or absolutely unstable. In all cases, the disturbance amplitudes are normalised by setting the maximum value at time $\tau = \pi$ to be unity, to allow comparisons to be made across different numerical simulations. Because a very wide range of magnitudes is found for the disturbance structures, a logarithmic n-factor is deployed to specify the contour levels as $n = \ln |\zeta(x, 0, \tau)|$, which highlights the exponential character of the growth. It should be noted that disturbances below a certain threshold are discounted in the contour plots, to ensure a clear and distinct depiction of the wavepacket locations within the spatial-temporal plane. This means that there are expansive regions where the disturbance is not shown because it has a very small magnitude. Wavepackets can sometimes thus appear as though they were completely detached from one another; when in fact the disturbance simply extends to each new location at a magnitude below the cut-off.

III. PURE STOKES LAYER

We first consider numerical simulation results for perturbations to the pure Stokes layer; i.e. for the case $\delta = 0$ in equation (2). To assist with our exposition, we will provide a brief review of the primary features of the family-tree-like disturbance structure that was discovered previously [1]. The spatial scaling of this structure with the Reynolds number is studied and shown to amount to a simple proportionality. The longer time disturbance development is then analysed and the existence of an absolute form of instability is demonstrated for the first time.

It may be noted that, as a validation of our newly developed numerical scheme, the particular cases exemplified in figures 1 and 2 from reference [1] were carefully reproduced. Following this, and a number of other stringent validity checks [17], we were able to extend our results to achieve very much longer simulation times than had proved possible before.

A. Family-tree-like structure

Figure 1(a) depicts the spatial-temporal contours of the wall vorticity perturbation field for the impulse response found at $Re = 700$, over the first three periods of wall motion. The corresponding development established when $Re = 750$ is plotted in figure 1(b). As was noted earlier, it is convenient to always choose the impulse to be centred about $x = 0$. Since the critical Reynolds number for the instability of Floquet modes [3] takes the value $Re_c = 707.84$, the first contour plot displays a marginally subcritical case, while the second is for a disturbance that is expected to be strongly unstable. Both of these illustrations depict the family-tree-like structure, where

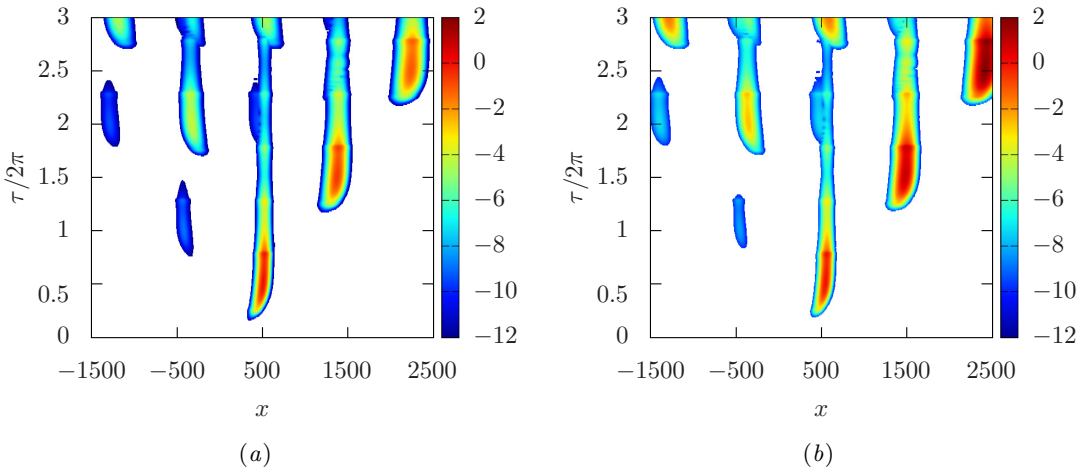

FIG. 1. Spatial-temporal contour plots of $n = \ln|\zeta(x, 0, \tau)|$, the logarithmic n-factor determined from the perturbation wall vorticity, for the first three periods of wall motion. (a) $Re = 700$; (b) $Re = 750$.

multiple wavepackets are triggered by a single impulsive excitation. It is noted that, since we have only plotted the magnitudes that define the envelopes of the disturbance, the wavelike spatial variation that is found within each of the wavepackets is not made evident. This smaller-scale spatial variation is of little consequence in a discussion of the larger-scale family-tree-like structure and convective/absolute instability.

At the earliest times considered, the oscillatory bounding wall moves towards positive x, which accounts for the initial convection of a disturbance wavepacket along the same direction. This original wavepacket is termed the *mother* wavepacket and is generated at the location of the wall-forcing, though the early development is at magnitudes below the low-amplitude cut-off and so does not appear in the contour plots. Within each period of the wall oscillation, two *daughter* wavepackets are generated that propagate either side of the mother wavepacket, each created half a time period apart from one another. The daughter wavepackets then birth two *grand-daughter* wavepackets per period, and so on. As time advances, there are instances where one or more wavepackets are observed to overlap with an existing wavepacket.

In both figures $1(a)$ and $1(b)$ the disturbance maximum progresses in the direction of positive x, moving through a succession of different wavepackets. More generally, the preferred propagation direction of the maximum amplitude of the perturbation is dictated by the phase of the time at which the impulsive forcing is applied within the time-periodic flow [1]. The maximum of the disturbance depicted in figure $1(a)$ decays as it passes from mother wavepacket to daughter wavepacket (located to the right of the mother), while the disturbance maximum grows in figure $1(b)$. This is consistent with the fact that $Re < Re_c$ for the first case and $Re > Re_c$ for the second.

A close inspection of the patterns formed by the disturbance boundaries shown in figure 1 reveals that the distances between neighbouring wavepackets become greater when the Reynolds number is increased. A measure of the distance between neighbouring wavepackets, denoted Λ, was computed by tracing the location of the disturbance maximum, which jumps from mother wavepacket to daughter wavepacket and so on. Values were determined for a selection of time instants, and their averages taken. These are plotted against Re in figure 2. Linear regression was applied to

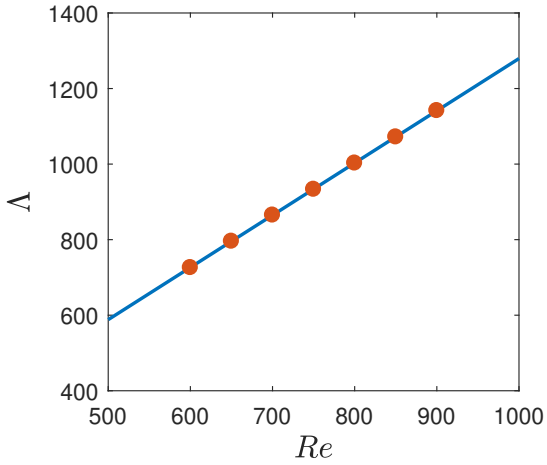

FIG. 2. Streamwise distance Λ between neighbouring wavepackets as a function of Re.

find the line of best fit, which is shown as a solid straight line with a constant of proportionality $d\Lambda/dRe = 1.38$. This simple kind of scaling behaviour can be attributed to the fact that the base flow is expected to transport disturbances by distances of $\mathcal{O}(Re)$ during each oscillation period; there is a factor of Re between the convective terms and the time derivative in the governing equations (5a) for the perturbation vorticity.

B. Absolutely unstable behaviour

Previously conducted numerical simulations of the impulse response for the pure Stokes layer [1] were only able to investigate the disturbance development for the first three periods of the oscillatory wall motion. This did not suffice to establish whether the flow instability was absolute rather than convective in nature. Asymptotic values for growth rates could be accurately determined at the non-stationary positions taken by the disturbance maximum. However, this proved not to be possible for the measurement of the growth at fixed spatial points, because transient initial behaviour remained significant. The deployment of our more efficient numerical scheme, in conjunction with the availability of greater computational resources, has allowed us to undertake simulations over twenty or more periods of the wall motion. The evolution of the family-tree-like structure could thus be studied in a far more comprehensive manner, permitting the extraction of converged values for the large-time rates of pointwise growth.

An extended spatial-temporal contour plot for the impulse response at $Re = 750$ is displayed in figure 3, ranging over the first ten periods of the wall motion. The largest values of the amplitude may be traced to the wavepackets that are formed and convected furthest to the right. However, if attention is focussed on the remainder of the disturbance structure, some other salient features are readily identified that persist even as this feature is convected out of the region of interest. Upon eliminating the most amplified wavepackets at the outer right of the disturbance structure, a 2Λ spatial periodicity can be seen between pairs of the remaining wavepackets that achieve a comparable magnitude. For instance, at time $\tau/2\pi = 4$, there are three wavepackets of almost equal amplitude that form at a distance 2Λ apart. However, at $\tau/2\pi = 5$ these particular wavepackets have

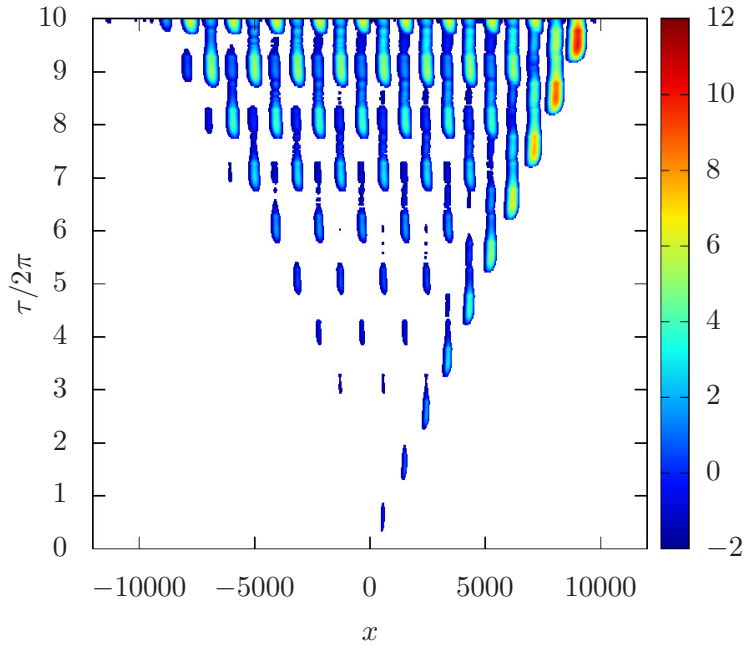

FIG. 3. Spatial-temporal contour plots of the logarithmic n-factor for the perturbation wall vorticity, showing the development over the first ten periods of wall motion for $Re = 750$.

decreased in magnitude and are now below the low-amplitude threshold of the illustration. Instead, four new equally sized wavepackets have developed, again with a 2Λ separation between them, but shifted by a streamwise distance $\pm\Lambda$ from the wavepackets observed during the previous period. A full period of wall motion later, the wavepackets that were present at $\tau/2\pi = 4$ have reappeared, at about the same streamwise positions, and attained a larger amplitude. On the other hand, the wavepackets found at $\tau/2\pi = 5$ are once again below the low-amplitude cut-off, but reappear again at $\tau/2\pi = 7$ with an even greater magnitude. This pattern of disturbance development continues to recur for the remaining time duration, and leads to the distinctive regularity in the wavepacket distribution that is exhibited in the figure. Wavepackets of comparable magnitude form at 2Λ streamwise intervals and increase in magnitude every two full cycles of wall motion. It may be inferred that there is an absolute form of instability, because accumulating temporal growth can be traced at fixed streamwise positions, over successive periods of the base flow oscillation.

Figure 4 provides a further illustration of the absolute instability. It displays the streamwise positions of the local n-factor maxima, denoted $n_{\max}$, for wavepackets of comparable magnitude. Those wavepackets located furthest to the right in figure 3, that encompass the disturbance maximum, have been removed from figure 4 to highlight the symmetric structure of the remaining wavepackets (we reiterate that the outer layer of wavepackets, on the right in figure 3, are a direct consequence of the time at which the localised impulsive wall forcing has been applied, so the disturbance maximum would propagate to the left if the wall excitation was delayed by half a period). The values taken at these maxima are plotted for a series of later instants of time, separated by the period of the wall motion. Thus the regularity in the wavepacket distribution is again depicted, though

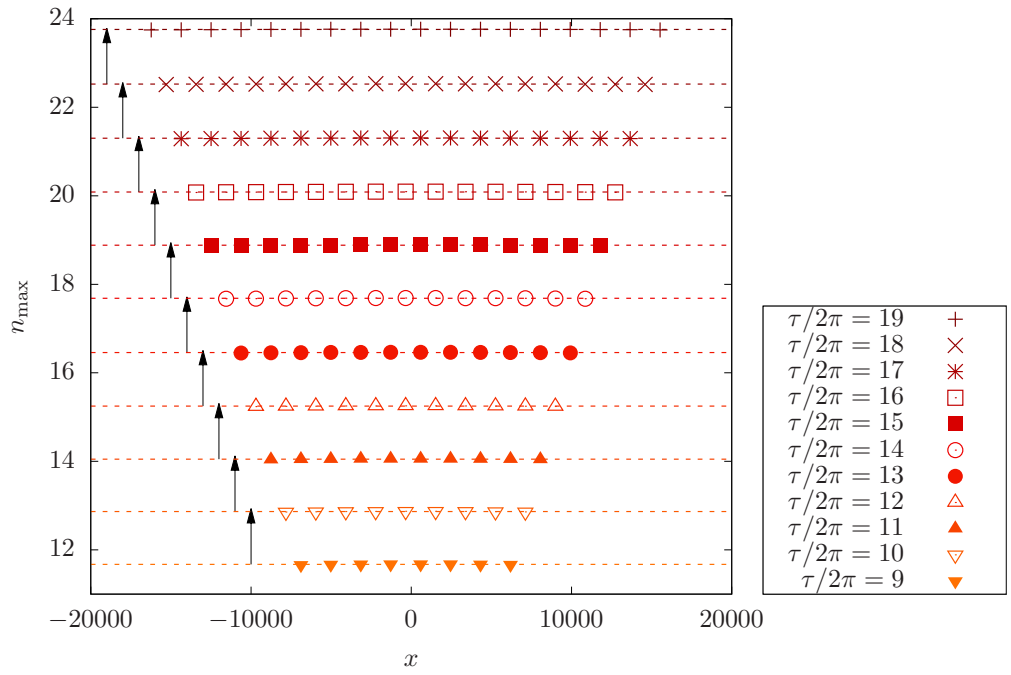

FIG. 4. Local n-factor maxima, $n_{\max}$, plotted against the corresponding streamwise x-location for the wavepackets displayed in figure 3 (excluding the outer wavepacket). Dashed horizontal lines indicate the mean value, $\bar{n}_{max}$, while arrows of length $\Delta n_{\max} = 1.26$ illustrate the almost constant increase in $\bar{n}_{\max}$ per period.

in a more schematic manner. The staggering that occurs between successive oscillation periods is highlighted, as is the 2Λ spatial periodicity between neighbouring wavepackets of a similar size. Furthermore, the pointwise temporal growth may be readily discerned. Vertical arrows of length $\Delta n_{\max} = 1.26$ have been drawn to illustrate that $\bar{n}_{\max}$, the average value at each time, increases at an almost constant rate between each of the time periods.

It may be surmised that the temporal variation at each fixed streamwise location is similar to that specified by the Floquet form (10), but restricted to the special case where there is an overall temporal periodicity with twice the period of the basic state; i.e. 4π-periodic. This period-doubling can be achieved by selecting the Floquet exponent to have a half-integer-valued imaginary part, so that, without loss of generality, it takes the form $\mu = \mu_r + i/2$. The duration of the time-periodicity contributed by the function f that appears in (10) is then effectively doubled and the temporal behaviour exhibited at each spatial point can be described as being *subharmonic*. Evidently, the numerical value determined for $\Delta n_{\max}$ may be used to provide an estimate for the real part of the Floquet exponent.

The strength of the absolute instability can be quantified using the pointwise growth rates μ_0 calculated from (12). These are plotted in figure 5, for the same disturbance at $Re = 750$ that was considered before. The growth rates were determined for three fixed streamwise locations, and sampled at the end of each time period of the wall motion. A plot of the temporal growth rate μ_m associated with the disturbance maximum, computed using (11), is also included. It may be seen that the pointwise growth rates at all of the chosen streamwise locations approach the same positive

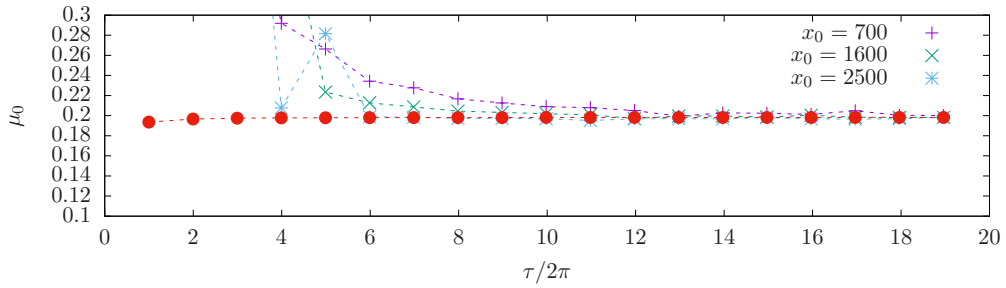

FIG. 5. Time-sampled values of the pointwise growth rates μ_0, measured at three different streamwise locations x_0. Dotted markers (•) denote the temporal growth rate μ_m associated with the disturbance maximum.

constant, exactly as would be anticipated for an absolutely unstable flow. Moreover, the temporal growth rate of the disturbance maximum asymptotes towards the same value. This eventual display of spatial uniformity in the measured temporal growth rates is not transparent from the behaviour during the first three periods of the wall motion (see figure 1), where the pattern of subharmonic growth is only beginning to emerge. Figure 5 shows that although the growth rate associated with the disturbance maximum converges towards an asymptotic value within the first three periods of wall motion, the growth rates measured at the fixed streamwise positions only start to converge after several more periods have passed.

For all of the Reynolds numbers that we considered, the pointwise growth rates and those determined by tracing the disturbance maximum were found to approach the same value, or at least a numerically very similar one. In particular, this held for cases near to the critical Reynolds number for the first appearance of the Floquet form of instability. Such concurrence suggests that the onset of absolute instability coincides with that of the Floquet instability [17].

The claim that the Floquet instability takes an absolute form as soon as it sets in can also be supported in a more straightforward fashion. A simple linear extrapolation between the asymptotic values of the pointwise growth rates μ_0 obtained for $Re = 700$ and $Re = 750$, which are listed in Table I, predicts a value of the critical Reynolds number for the onset of absolute instability that matches the value of $Re_c = 707.84$ for the onset of Floquet instability to within 0.1%. Nevertheless, it cannot be concluded that the pure Stokes layer can only ever be absolutely unstable, since it is conceivable that convectively unstable disturbances might still be found at supercritical values of Re. However, no evidence of such behaviour was discovered for any of the disturbances that we examined.

It is important to emphasise that the spatial periodicity observed here is a persistent feature of the disturbance development, even as the global maximum convects away in the wavepacket furthest to the right (much like a convective form of instability). The growth-rate associated with the disturbance maximum is identical to that found about fixed spatial locations. Furthermore, the direction in which the wavepacket containing the maximum convects is reversed by exciting the flow when the plate is travelling in the opposite direction. Thus, the larger magnitude of the outer layer is a manifestation of the phase of excitation rather than an underlying feature of the impulse response.

	1(*a*)	1(*b*)	7(*a*)	7(*b*)	7(*c*)	7(*d*)	7(*e*)	7(*f*)
δ	0	0	0.0002	0.0008	0.0012	0.002	0.005	0.01
Re	700	750	750	700	650	600	550	500
μ_m	-0.0416	0.1982	0.2050	0.1545	0.2432	0.4019	0.7723	0.8441
μ_0	-0.0374	0.2001	0.1977	0.1523	0.2376	0.3992	0.7708	0.8413

TABLE I. Asymptotic values of the temporal growth rates μ_m and μ_0 for the disturbances depicted in figures 1 and 7.

IV. MODIFIED STOKES LAYER

The scope of the numerical simulations is now broadened to include oscillating flows with a low-amplitude, high-frequency harmonic; i.e. $\delta \neq 0$ in (2). Since it was not feasible to explore the whole of the parameter set for this family of flows, the subsequent reports are restricted to the subset for which $(a_p, b_p) = (1, 0)$. Additionally, the disturbance development was only investigated for a limited set of high-frequency harmonic numbers p. Evidence that similar stability features are to be found for alternative (a_p, b_p) combinations is provided in [17].

A. Destabilising effect of high-frequency harmonics

Figure 6 depicts the variation in the critical Reynolds number Re_c with the amplitude δ for $p = 50, 60$ and 70 (the high-frequency harmonic p selected to display disturbance development was guided by the earlier investigation of Thomas *et al.* [11] that observed a significant destabilisation for $35 \leq p \leq 105$). The critical Reynolds number for each δ and p combination was determined using the simulation data. Growth rates μ_m were computed for an extensive selection of values for Re, with measurements sampled at the end of ten periods of wall motion. This was deemed to be sufficiently long for the growth rates to have achieved a good approximation to their asymptotic values. A bisection method was then utilised to find the critical Reynolds number Re_c corresponding to zero net growth. For all three chosen values of the harmonic frequency that were considered, there is initially a steep reduction in Re_c. However, for $\delta \gtrsim 0.006$, the onset of instability is less affected by further increases in the amplitude of the high-frequency harmonic. Nevertheless, significant destabilisation is still realised; for $p = 70$ and $\delta = 0.01$ the critical Reynolds number is brought down to less than half of the value for the pure Stokes layer. The sudden change in the gradient near $\delta = 0.0016$ in the curve for $p = 70$ is the manifestation of a change in the least-stable mode [17]: For $\delta < 0.0016$, the neutrally stable mode is characterised by wavenumbers $\alpha \sim 0.4$, whereas for $\delta = 0.0016$, a distinct mode with $\alpha \sim 0.3$ becomes less stable than the higher-α mode. As δ increases further, the neutrally stable modes continue to correspond to $\alpha \sim 0.3$.

B. Disruption of the family-tree-like structure

Spatial-temporal contour plots are constructed in figure 7 for six combinations of the parameters Re and δ, with the high-frequency of the harmonic held at $p = 60$. Perturbations are once again

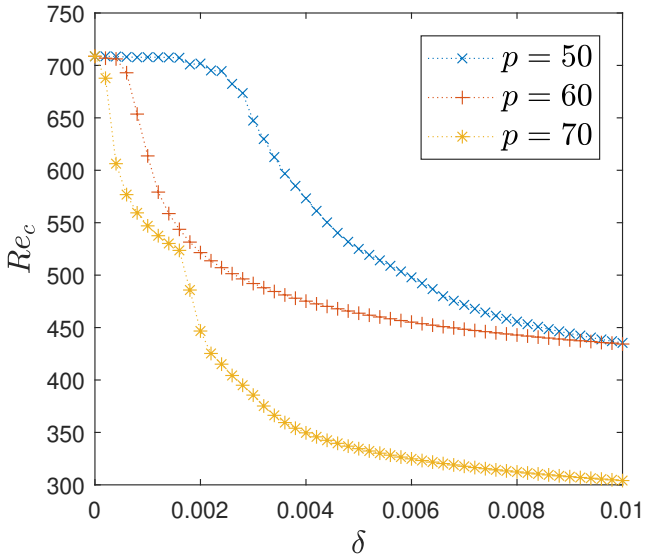

FIG. 6. Variations in Re_c with δ for $p = 50, 60$ and 70.

excited using an impulsive forcing centred at $x = 0$ and the response is displayed for the first three full periods of wall motion. The parameter combinations, tabulated in table I, were carefully chosen to illuminate the change in behaviour as the amplitude of the harmonic was increased. In each instance, the asymptotic temporal growth rate μ_m, as determined from the recipe (11) at a sufficiently large time, is within the range $0.15 < \mu_m < 0.85$. Hence, all of the considered disturbances are unstable. Moreover, there is clear evidence of the destabilising effect brought about by the inclusion of the high-frequency harmonic, since strongly unstable disturbances develop at significantly lower Reynolds numbers as the amplitude δ is increased.

The six contour plots depicted in figure 7 illustrate that as δ increases, the family-tree-like structure breaks down. The multiple wavepacket formations are progressively replaced by what is better described as being a structure that is dominated by the recurrent appearance of a single wavepacket. This seems to propagate in alternating directions, as it responds to the reversals of the basic state flow over the cycle of wall motion. A more refined description of the sequence of changing behaviour will be given below.

In figure 7(a), where $\delta = 0.0002$, the disturbance develops in a manner that is broadly comparable with what was observed for the pure Stokes layer. This may be confirmed by referring back to figure 1. However, a new group of *secondary* wavepackets emerge at about the same points in time as the daughter wavepackets. These are located immediately adjacent to the mother wavepacket. For instance, it may be seen that around $\tau/2\pi = 1.5$, a lower-amplitude wavepacket (labelled S), discernible by its lighter tone, is formed to the right of the mother wavepacket (M), but to the left of the daughter wavepacket (D). Increasing the amplitude of the harmonic to $\delta = 0.0008$, as is shown in figure 7(b), establishes secondary wavepackets with amplitudes that are in excess of those of the daughter and granddaughter wavepackets. Thus, the disturbance maximum is no longer transmitted from the mother wavepacket to the daughter wavepackets. Instead, the maximum amplitude passes from the mother wavepacket to the secondary wavepackets.

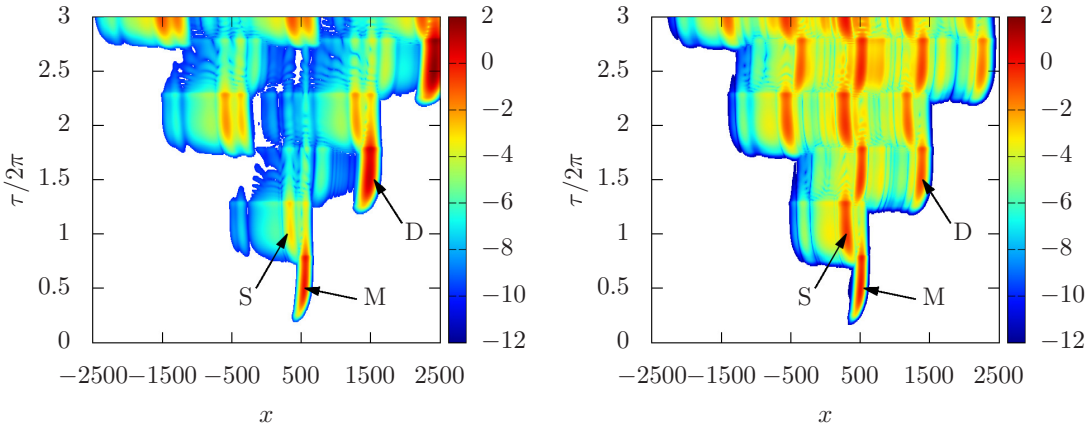

(*a*) $\delta = 0.0002,\ Re = 750$ (*b*) $\delta = 0.0008,\ Re = 700$

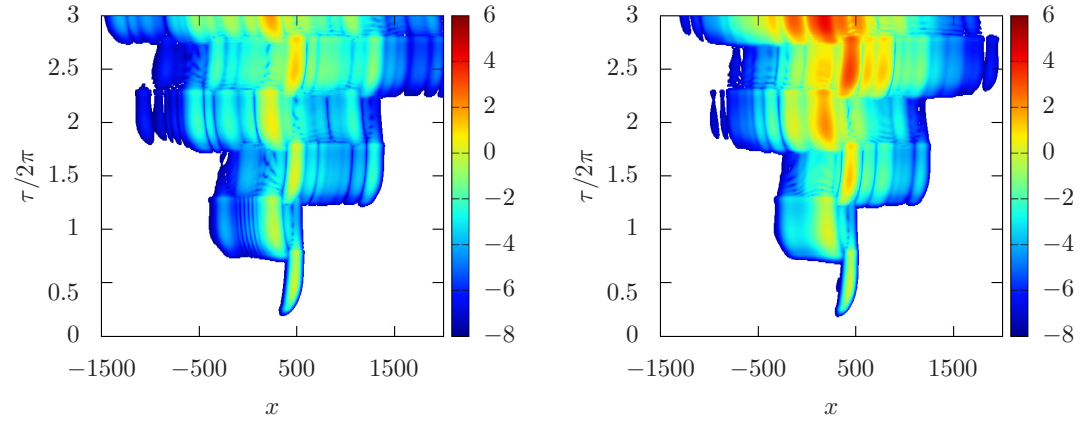

(*c*) $\delta = 0.0012,\ Re = 650$ (*d*) $\delta = 0.002,\ Re = 600$

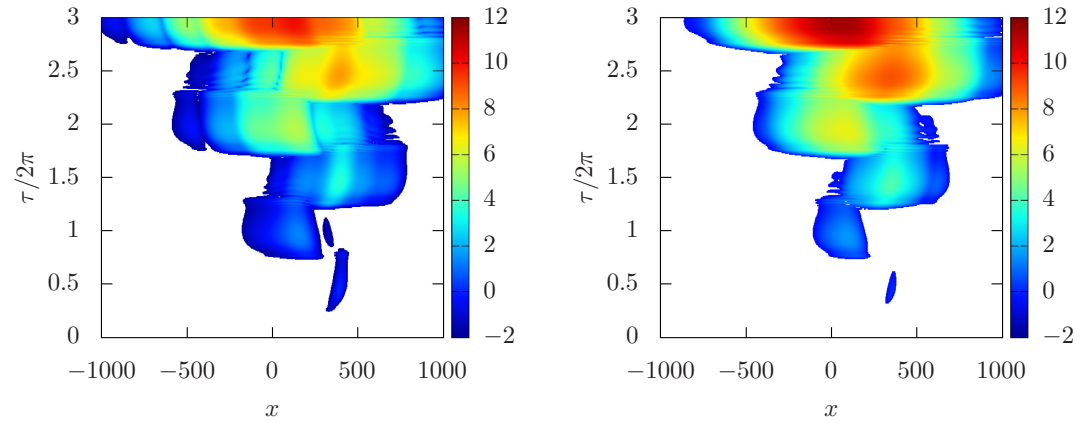

(*e*) $\delta = 0.005,\ Re = 550$ (*f*) $\delta = 0.01,\ Re = 500$

FIG. 7. Spatial-temporal contour plots of the logarithmic n-factor of the perturbation wall vorticity, for $p = 60$ and six combinations of Re and δ. In (*a*) and (*b*) the initial mother wavepacket is labelled 'M', with the corresponding daughter and secondary wavepackets labelled 'D' and 'S', respectively.

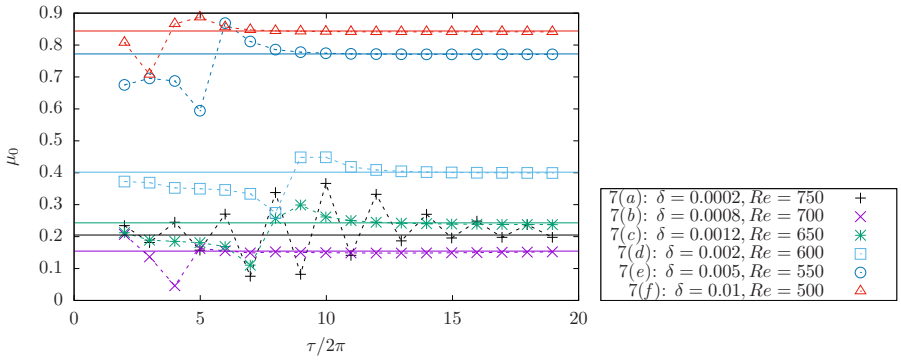

FIG. 8. Time-sampled values of the pointwise temporal growth rates μ_0 measured at $x_0 = 200$, for the six disturbances illustrated in figure 7. Solid lines indicate the asymptotic values of the growth rate μ_m based on the disturbance maximum, which are also tabulated in table I.

When δ is increased to take larger values, as illustrated in the sequence of figures 7(c)-(f), the daughter and granddaughter wavepackets become less and less distinct. If δ becomes large enough, then the family-tree-like structure is replaced by the previously mentioned single alternating wavepacket formation; as shown in figure 7(f). This suggests that the family-tree-like structure that develops in the pure Stokes layer is unlikely to be observed in any physical experiment that is configured in a similar manner to those which have been conducted to date. As we mentioned previously, the reported noise [7, 9] reached amplitudes that were of the order of 1% of the driving wall motion, which would notionally correspond to $\delta \sim 0.01$.

The changes in the disturbance structure, when δ increases, transform the qualitative nature of both the spatial and the temporal behaviour. Figures 7(b)-(f) show that the 2Λ spatial periodicity, which had previously been noted to develop between neighbouring equally sized wavepackets, becomes replaced by a Λ spatial periodicity. This can be traced to the formation of increasingly dominant secondary wavepackets. Furthermore, the subharmonic pattern of temporal growth that was displayed for the pure Stokes layer appears to be supplanted by a *harmonic* form of growth, where the wavepacket arrangement may be construed as reasserting itself every period of wall motion, rather than every two. Such behaviour can be described by a special case of the Floquet mode form (10) which displays an overall 2π-periodicity. This is achieved by selecting the Floquet exponent μ to have a vanishing imaginary part, so that $\mu = \mu_r$ as opposed to the choice $\mu = \mu_r + i/2$ that was needed for the subharmonic case. One consequence of the change in the nature of the temporal variation from subharmonic to harmonic is that, for the disturbances plotted in figures 7(c)-(f), clear evidence for the presence of an absolute instability can be discerned within the first three periods of the wall motion: When following the progress of the disturbance along any vertical line, we observe temporal growth across successive periods.

Closer inspection of the disturbance structures depicted in figure 7 suggests that there is, in fact, absolute instability in all six cases. Support for this claim is provided in figure 8, which displays time-sampled values for the pointwise growth rates, computed at a chosen spatial location. The corresponding large time asymptotic values are tabulated in table I. In each instance, the pointwise growth rate converges to a positive value that is visually indistinguishable from the asymptotic growth rate determined by considering the disturbance maximum. The computed values for the latter are marked using solid horizontal lines. It may be surmised that sustained temporal growth is being exhibited in every case.

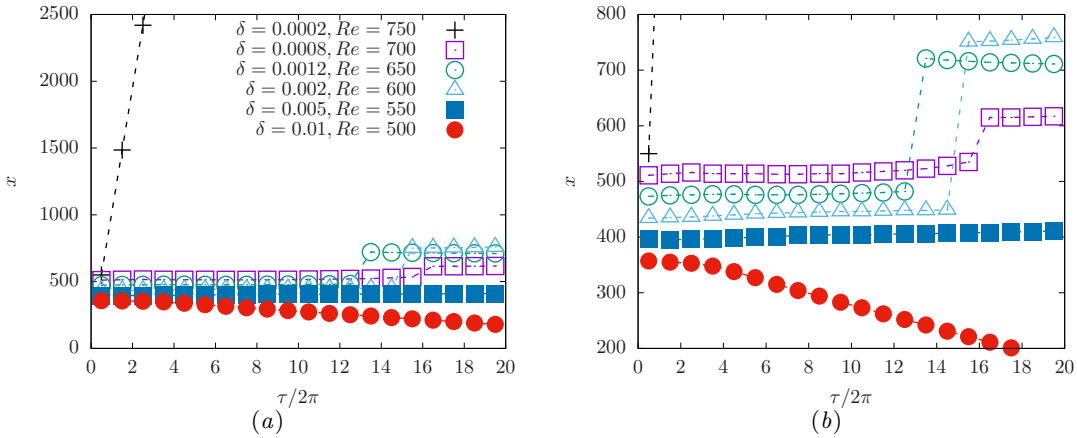

FIG. 9. Sampled time variation of the streamwise location of the disturbance maximum, for the disturbances depicted in figure 7. (a) plotted over a wider range of locations; (b) using a reduced range, to better illustrate the behaviour corresponding to the cases shown in figures 7(b)-(f).

C. Different regimes for absolute instability

To identify some further features of the absolutely unstable behaviour, we consider the progression of the disturbance maximum. This is represented in figure 9, for each of the cases that were previously illustrated in figure 7. The streamwise location of the maximum is tracked for time instants at the mid-points of successive oscillation periods. Three different regimes of behaviour can be distinguished.

In the first regime (I), the disturbance retains the family-tree-like structure found for the pure Stokes layer. As might be expected, this is the case when the amplitude δ is kept sufficiently small, as in figure 7(a). The disturbance maximum shifts towards larger x, progressing by a distance of $\mathcal{O}(Re)$ during each period of the wall motion. This relatively rapid form of relocation is evidenced by the steeply sloped line that is displayed on the far left in figure 9(a).

As the harmonic amplitude δ is raised to larger values, two new regimes may be identified, which are both associated with a reduction in the movement of the disturbance maximum. The second regime (II) encompasses those disturbances that were illustrated in figures 7(b)-(d). In all of these instances, the disturbance maximum initially remains located in what was previously described as the mother wavepacket. From figure 9(b) it may be discerned that although the maximum stays there for many periods of the wall motion, it eventually jumps to a new streamwise position, located at a higher value of x. In each case modelled, the abrupt change in location takes place during a different time period.

The third regime (III) characterises the disturbances shown in figures 7(e)-(f), where the family-tree-like structure has completely broken down. This is replaced by a structural formation that involves only a single wavepacket, which re-emerges every half time period and appears to propagate along alternating directions. The data plotted in figure 9(b) shows that, for the earliest of the periodically sampled time instants, the disturbance maximum can be found at an almost constant location. However, over the course of many more time periods, it slowly moves away. Although this movement is not very obvious in the plot for the case that corresponds to figure 7(e), the maximum can be clearly seen to propagate in the negative x-direction for the perturbation depicted

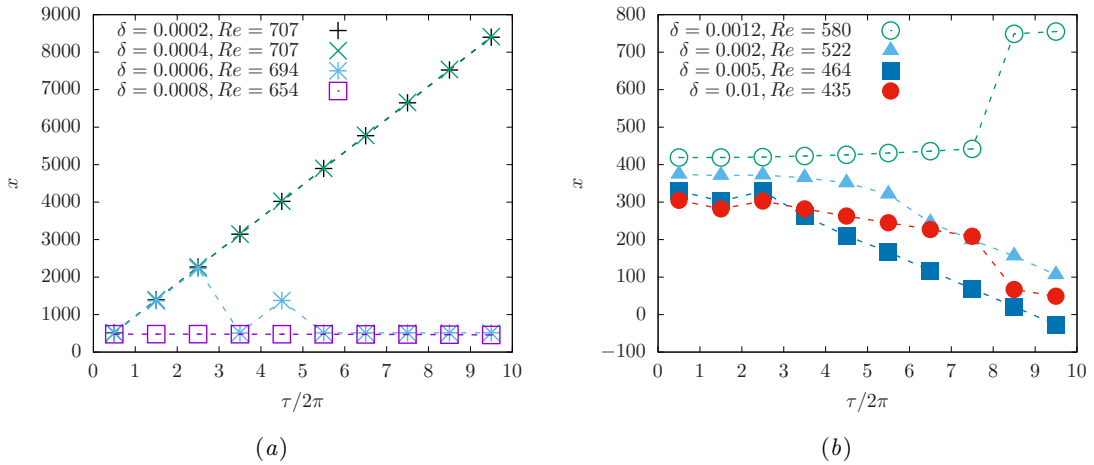

FIG. 10. Sampled time variation of the streamwise location of the disturbance maximum, for a selection of marginally unstable disturbances. (a) Small-valued δ and (b) larger-valued δ. Open and filled symbols indicate whether a disturbance belongs to regime II or III, respectively.

in figure 7(f).

While the distinct behaviours are evident in figure 9, some additional cases were considered to better demonstrate the transitions between the three regimes. In figure 10(a), the transition from regime I to II is documented over four marginally unstable cases. For noise amplitudes $\delta = 0.0002$ and 0.0008, behaviour associated with regime I and II is observed, respectively. Similar observations were identified in figure 9 for these particular values of δ but at higher Reynolds numbers Re, suggesting that the transition between these two regimes is primarily controlled by δ. The case corresponding to $\delta = 0.0004$ also belongs definitively to regime I; the wavepacket spacing matches that for $\delta = 0.0002$ since $Re = 707$ in both instances. The behaviour associated with case $\delta = 0.0006$ is more complicated. Initially, the wavepacket furthest to the right is dominant and regime I behaviour is observed. However, by the end of the time interval shown the original mother wavepacket is dominant and regime II behaviour is realised. This indicates that the transition from regime I to II is populated by cases in which the daughter and secondary wavepackets are of similar size but one eventually dominates. It should then be possible to find a value of δ for which the daughter and secondary wavepackets match in magnitude indefinitely, though in practise this would be difficult to determine through numerical simulations alone.

Figure 10(b) depicts the evolution of the location of the maximum for marginally unstable disturbances with δ matching those cases shown in figure 7(c-f). In most instances, the regimes are identical to those equivalent δ-cases illustrated in figure 9. While it might be concluded from figure 9 that regime III behaviour is associated with larger growth-rates μ_m than regime II behaviour, the reduction in the Reynolds number Re for the marginal cases ($\mu_m \gtrsim 0$) depicted in figure 10 does not correspond to a transition from regime III to II behaviour. In fact, the cases corresponding to $\delta = 0.0012$ and $\delta \geq 0.005$ consistently belong to regimes II and III, respectively. Moreover, when $\delta = 0.002$, the marginally unstable case depicted in figure 10(b) belongs to regime III, whereas the strongly unstable case depicted in figure 9 belongs to regime II. Therefore, we conclude that unlike the transition between regimes I and II (which appears to be controlled entirely by δ), there is a subtle transition between regimes II and III in which the Reynolds number Re (and consequently

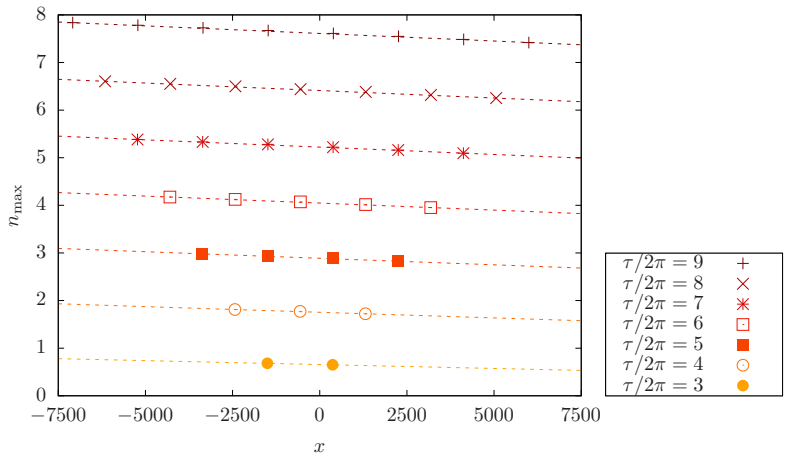

FIG. 11. Local n-factor maxima, displayed in a similar fashion to that used for figure 4, but for the disturbance depicted in figure 7(a) with $Re = 750$, $\delta = 0.0002$ and $p = 60$. The dashed straight lines are drawn through the locations of the outermost maxima at each of the chosen time instants.

the growth-rate μ_m) plays an important but complex role. Intriguingly, the distance travelled by the disturbance maximum in all of those marginally unstable cases considered in figure 10 is significantly greater than the corresponding cases plotted in figure 9, despite the simulations being run for half the number of cycles.

D. Directional symmetry breaking and anti-periodicity

For the pure Stokes layer, the disturbance development was marked out by regularities in the spatio-temporal arrangement of the wavepacket components. These were illustrated in a schematic manner in figure 4. A similarly constructed depiction is given in figure 11, for the modified Stokes layer configuration with $\delta = 0.0002$ and $p = 60$. This represents the same disturbance as was displayed in figure 7(a), which is classified to be within regime I where the family-tree-like structure persists. The n-factor maxima $n_{\max}$ attained by individual wavepackets (excluding the largest located furthest to the right) are plotted against the corresponding streamwise locations, for time instants between the third and ninth periods of the wall motion. It is immediately apparent that the wavepackets located on the left of the illustration attain larger $n_{\max}$ values than those that develop on the right. The disturbance can thus be interpreted as undergoing a spatial growth directed along the negative x-direction. In fact, as is indicated by the dashed straight lines that are drawn between the locations of the maxima displayed in the figure, the spatial growth is exponential and may be described by a factor of the form $\exp(-\lambda x)$ with $\lambda/\delta \simeq 0.15$. The persistent spatial structure of the disurbance, as illustrated in figure 11, is no longer symmetric, even with the omission of the wavepacket furthest to the right.

Although the inclusion of a high-frequency harmonic has led to an asymmetric modification of the wavepacket pattern, other features that were found for the pure Stokes layer are retained. A fixed streamwise spacing is still kept between neighbouring wavepackets, and a subharmonic form of pointwise growth is once again evident. The near constancy of the pointwise determined temporal growth for all of the maxima depicted in figure 11 is demonstrated by the almost equal spacing and

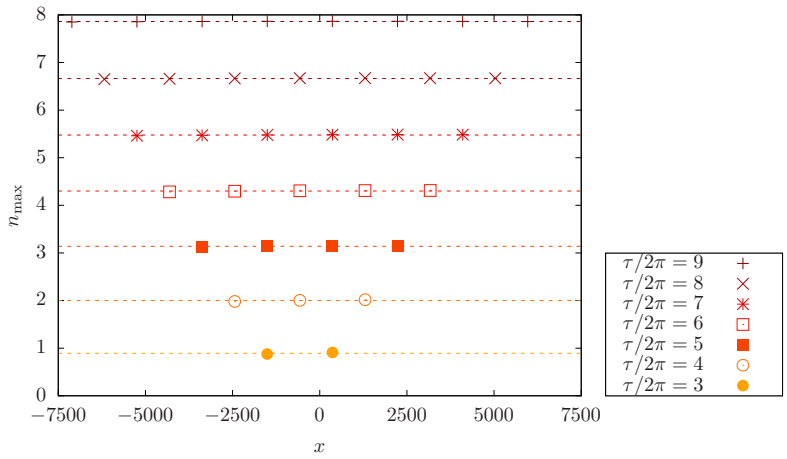

FIG. 12. Local n-factor maxima, displayed in the same manner as in figure 11, for a disturbance developing in a base flow where the harmonic number is changed to $p = 61$. As before, $Re = 750$ and $\delta = 0.0002$. The dashed horizontal lines now indicate the average value, $\bar{n}_{\max}$, at each time.

parallel nature of the exhibited dashed lines. The wavepacket maxima recur at the same spatial locations every two time periods, with amplitudes that grow by the same increment in n_{max}. This asymptotes to μ_0/π, where μ_0 is the pointwise growth rate which takes the value stated earlier in table I.

The development of asymmetry with respect to the x-direction can be attributed to a violation of the *anti-periodicity* of the oscillatory basic state. The pure Stokes layer reverses its flow direction every half period and then retraces exactly the same time variation as before, but with the opposite orientation. This means that no fundamental distinction can be made between the positive and negative x-directions (except for in the timing of the excitation manifesting in the larger magnitude of wavepackets in the outer layer). However, the addition of an harmonic with an even value of p leads to a basic state (2) for which $U_B(y, \tau + \pi) \neq -U_B(y, \tau)$. Thus the argument that establishes that the positive and negative x-directions must be equivalent no longer holds. The significance of this may be further attested by examining a slightly amended configuration where $p = 61$, with the Reynolds number and the amplitude of the harmonic held unchanged from the previous case for $p = 60$. As with all odd-numbered harmonics, the anti-periodicity of the basic state is then preserved. It can be confirmed from an inspection of figure 12 that, as expected, the disturbance pattern no longer loses its symmetry.

Having discussed the effect of the anti-periodicity of the basic state on the symmetry of the disturbance development for a case where the family-tree-structure remains intact, we now briefly describe how similar alterations can be traced when this structure is strongly disrupted. For a selection of harmonically modified base flows, Figure 13 exhibits the progression of the streamwise location where the response to the impulsive excitation achieves its maximum. The times are once more sampled at the mid-points of the wall motion oscillation periods. Results are shown for two distinct sets of the parameters Re and δ, and for a range of even and odd numbered high-frequency harmonics. These were chosen to illustrate the behaviour that arises within regime III, where the disturbance maximum remains relatively near to the origin of the impulsive forcing. In all of the instances considered, the maximum is initially found at approximately the same streamwise location. However, for the base flows which incorporate an even numbered high-frequency harmonic

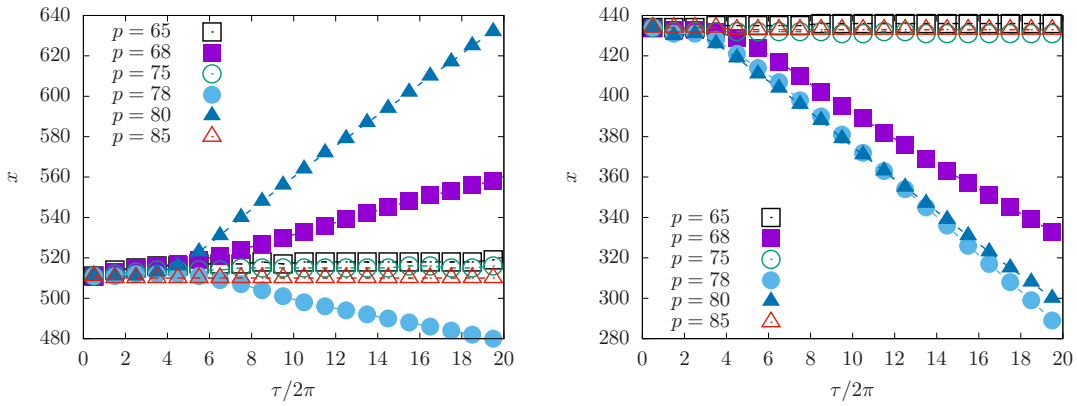

FIG. 13. Progression of the streamwise location of the disturbance maximum over time, for a selection of high-frequency harmonic numbers p. (a) $Re = 700, \delta = 0.001$; (b) $Re = 600, \delta = 0.005$. Odd values of p are represented by open symbols while even values are represented by closed symbols.

p, a clear unidirectional motion is eventually exhibited. This remains relatively slow, in comparison with the $\mathcal{O}(Re)$ displacement that can be achieved over each time period for the wavepackets that develop when a family-tree-like structure is formed. Nevertheless, there is still a marked contrast with what is found for the flows with an odd value of p. For the latter case, it can be seen that the disturbance maximum remains almost fixed at about the same location for the entire time duration that is considered. The existence of these two distinct forms of behaviour again attests to the significance of the violation or retainment of anti-periodicity in the basic state.

Intriguingly, the direction in which the disturbance maximum travels for even p is not consistent across the cases shown in figure 13. For flows of this type the mean flow over a period is zero, so there is no immediately obvious mechanism for this convection. This observation reinforces the implicit assumption that for the regime II and III disturbances depicted in figure 13, the changing location of the disturbance maximum reflects an asymmetry in the wavepacket structure that is independent of the time at which the localised impulsive wall forcing is applied and holds across all streamwise locations x and time τ. This is distinct from the regime I disturbances in which the behaviour of the disturbance maximum is dictated entirely by the excitation regardless of whether the wavepacket structure is spatially symmetric (figures 4 and 12) or if this symmetry has been broken (figure 11).

V. CONCLUSIONS

A numerical investigation has been undertaken of the spatio-temporal development of linearized disturbances in the pure Stokes layer and the family of oscillating flows that is obtained through its modification by a low-amplitude, high-frequency harmonic. Combining the novel numerical methods of [15] with a spectral treatment of the streamwise variation, the impulse response was studied for many more periods of the wall motion than had previously been possible [1].

Significant new features of the family-tree-like pattern of the disturbance development were identified for the pure Stokes layer. In particular, it was discovered that unstable disturbances establish

a staggered wavepacket formation, with a subharmonic form of temporal periodicity displayed at fixed spatial positions. It was also demonstrated that the pure Stokes layer is absolutely unstable, with the onset of absolute instability coinciding with the critical Reynolds number obtained from Floquet theory.

The effects of incorporating a high-frequency harmonic into the basic state were systematically investigated. It was confirmed that even a very small level of harmonic modification can bring about a marked reduction in the critical Reynolds number for the onset of linear instability [11]. When the amplitude of the harmonic was kept sufficiently low, the disturbance development retained a family-tree-like structure and a subharmonic form of temporal behaviour. However, spatially asymmetric wavepacket patterns were observed in instances where the high-frequency harmonic number p was taken to be even. This was attributed to a breakdown of temporal anti-periodicity in the basic state. Changes in the disturbance behaviour were also correlated with violations of anti-periodicity for cases that involved higher amplitude harmonics.

Increasing the level of harmonic alteration to the basic state was found to lead to a disruption of the family-tree-like structure for the disturbance development. The formation of multiple wavepackets is replaced by a much simpler form of behaviour, in which a dominant wavepacket emerges at alternating spatial locations. Furthermore, there is a qualitative change in the temporal behaviour exhibited at any given spatial point. The period doubling associated with a subharmonic type of development is supplanted by a temporal periodicity that matches that of the basic state. This has the consequence that, for higher amplitude modifications of the basic state, absolutely unstable behaviour is distinguishable at much earlier times than is the case for the pure Stokes layer.

It should be reiterated that the present work has focussed on the linearized development. A previous study of the pure Stokes layer [1] also included a brief investigation of nonlinear disturbances. Much of the behaviour that was found, such as the growth of structures with very small temporal and spatial scales, may be expected to remain pertinent when the basic state is modified by a high-frequency low-amplitude harmonic. Moreover, our demonstration that the pure Stokes layer is absolutely unstable as soon as it becomes linearly unstable implies that nonlinear forms of disturbance development are inevitable whenever the threshold for Floquest instability is exceeded. Our further discovery that absolute instability can emerge at substantially lower Reynolds numbers for the modified Stokes layers suggests that nonlinear behaviour would be promoted in physical experiments whenever there was a significant level of noise in the wall motion.

Finally, it may be mentioned that we have also undertaken a comprehensive analytical study for the same family of oscillatory flows as have been examined here [17]. The pinch-point method [12] was used to demonstrate the existence of absolute instability and determine its onset. This study will be reported upon separately. It led to the unforeseen discovery that there are in fact multiple modes of absolute instability, related to each other by small increments of the wavenumber.

ACKNOWLEDGMENTS

This work was supported by the UK Engineering and Physical Sciences Research Council. The authors wish to thank Dr. Peter Blennerhassett and Prof. Andrew Bassom for their valuable contributions at its outset. The simulations were conducted using the Advanced Research Computing Division (ARCCA) facilities at Cardiff University. The authors are grateful to the referees for

several suggestions which have led to a much improved paper.

---

[1] C. Thomas, C. Davies, A. P. Bassom, and P. J. Blennerhassett, Evolution of disturbance wavepackets in an oscillatory stokes layer, J. Fluid Mech. **752**, 543 (2014).

[2] P. Hall, The linear stability of flat Stokes layers, Proc. R. Soc. A **359**, 151 (1978).

[3] P. J. Blennerhassett and A. P. Bassom, The linear stability of flat Stokes layers, J. Fluid Mech. **464**, 393 (2002).

[4] J. Luo and X. Wu, On the linear instability of a finite Stokes layer: Instantaneous versus Floquet modes, Phys. Fluids **22**, 054106 (2010).

[5] C. Thomas, A. P. Bassom, P. J. Blennerhassett, and C. Davies, Direct numerical simulations of small disturbances in the classical Stokes layer, J. Eng. Math. **68**, 327 (2010).

[6] S. Morgan and C. Davies, Linear stability eigenmodal analysis for steady and temporally periodic boundary-layer flow configurations using a velocity-vorticity formulation, J. Comput. Phys. **409**, 109325 (2020).

[7] R. Akhaven, R. D. Kamm, and A. H. Shapiro, An investigation of transition to turbulence in bounded oscillatory flows. Part 1. Experiments., J. Fluid Mech. **225**, 395 (1991).

[8] M. Clamen and P. Minton, An experimental investigation of flow in an oscillating pipe, J. Fluid Mech. **81**, 421 (1977).

[9] D. M. Eckmann and J. B. Grotberg, Experiments on transition to turbulence in oscillatory pipe flow, J. Fluid Mech. **222**, 329 (1991).

[10] M. Hino, M. Sawamoto, and S. Takasu, Experiments on transition to turbulence in an oscillatory pipe flow, J. Fluid Mech. **75**, 193 (1976).

[11] C. Thomas, P. J. Blennerhassett, A. P. Bassom, and C. Davies, The linear stability of a Stokes layer subjected to high frequency perturbations, J. Fluid Mech. **764**, 193 (2015).

[12] L. Brevdo and T. J. Bridges, Absolute and convective instabilities of temporally oscillating flows, Z. Angew. Math. Mech. **48**, 290 (1997).

[13] C. Davies and P. Carpenter, A novel velocity-vorticity formulation of the Navier-Stokes equations with applications to boundary layer disturbance evolution, J. Comput. Phys. **172**, 119 (2001).

[14] C. Von Kerczek and S. H. Davis, Linear stability theory of oscillatory Stokes layers, J. Fluid Mech. **62**, 753 (1974).

[15] M. Togneri and C. Davies, A high order finite-difference solver for investigation of disturbance development in turbulent boundary layers, Comput. Fluids **46**, 472 (2011).

[16] S. K. Lele, Compact finite difference schemes with spectral-like resolution, J. Comput. Phys. **103**, 16 (1992).

[17] A. Ramage, *Linear disturbance evolution in the semi-infinite Stokes layer and related flows*, Ph.D. thesis, School of Mathematics, Cardiff University (2017).